Modeling the Coagulation of Charged Particles

P. Jiang*, J.S. Lighty, A.F. Sarofim, E. Eddings
Combustion Research Group
University of Utah
Salt Lake City UT 84112-1114

Abstract
One important mechanism in the growth of soot particles is to understand the role of particle charge in the coagulation of the particles. A previously developed model has been extended to include the coagulation of charged particles. The model includes neutral particles and charged particles (up to three charges). The enhancement factors for the coagulation between neutral and charged particles, and between like-charged particles, have been computed. These factors have been used in a computer code for simulating the coagulation of charged particles. The results included the predictions of the percentage of charged particles with different charges after the coagulation process. The simulation of the particle number and size evolution agrees well with published experimental data.

Introduction

It is well known that the addition of small amounts of substances of low ionization potential, such as alkali or alkaline earth metals, can greatly enhance ionization in the flame product gas; however, the effect of additives on flame ionization is very complex [1]. In experiments where metals were added to the flame by atomization of an aqueous solution of their salts, an increase in soot particle number [2] and a decrease of the soot particle size [2-4] resulted. Haynes et al [2] suggested that alkali metal ions transfer their charge to the incipient uncharged soot particles. The result is the electrostatic repulsion between the charged soot particles, and thus, their coagulation and coalescence are inhibited. Consequently, the addition of an alkali metal increases the final number of soot particles and also reduces their size [2,5].

Based on the qualitative analysis that the coagulation of charged particles is inhibited due to their repulsive electrostatic force [6-9] and the observations that certain amounts of soot particles are charged with positive polarity [6,8,10,11], efforts have been made to utilize this feature to control soot emissions. Studies on applying electric fields to sooting flames show a significant influence of these fields on the dynamics of the soot coagulation process [12]. A marked reduction in soot emissions and a decrease in particle size were also observed when DC or AC (14kHz) corona discharges were applied to a propane turbulent diffusion flame [13,14].

Since the soot particle coagulation process is affected by charged particles, a quantitative analysis of this effect is needed in order to have a better understanding of this process. An enhancement factor approach has been used to indicate the effects of charged particles on particle collision rate. The enhancement factor between a charged particle and a neutral particle, and between the oppositely-charged particles has been previously computed [15]. The enhancement factor for like-charged soot particles has been approximated by a simplified analysis that is only valid for the case of equal particle diameters [16, 17]. This approximate method has been used for simulating soot particle coagulation in low-pressure flames [18, 19]. A more precise methodology has been proposed by considering simultaneous van der Waals forces, Coulomb forces, and image forces for monotonic or non-monotonic potentials between particles [20, 21]. The goal of the present work is to simulate the coagulation of charged particles with multiple charges.

Model Development

The coagulation of charged particles is modeled based on a previously developed coagulation model [22].

In this model, we have four sets of bins (components): neutral particles; charged particles with one charge; charged particles with two charges; and charged particles with three charges. Charged particles with more than three charges were neglected. Previous analysis has shown that the average number of charges per particle is in the range of 1-3 [2].

The model shown in Figure 1 represents the physical process of coagulation when including charged particles. There are three basic types of coagulation events: (1) two neutral particles coagulate forming a larger neutral particle; (2) a neutral particle and a charged particle coagulate forming a larger charged particle with the same charge as the charged particle before coagulation; and (3) two charged particles coagulate forming a larger charged particle with the number of charges equal to the sum of

* Corresponding author: pjiang@eng.utah.edu
Associated Web site: http://www.combustion.utah.edu
Proceedings of the Third Joint Meeting of the U.S. Sections of The Combustion Institute

the number of charges of the two particles before coagulation.

In this model, six coagulation events can happen in parallel, i.e. the coagulation between: neutral and neutral particles (Event 1), neutral and charged particles with one charge (Event 2), neutral and charged particles with two charges (Event 3), neutral and charged particles with three charges (Event 4), charged particles with one charge and charged particles with one charge (Event 5), charged particles with one charge and charged particles with two charges (Event 6). The mathematical description of these simultaneous coagulation processes is given in next section. The model is shown in figure 1.

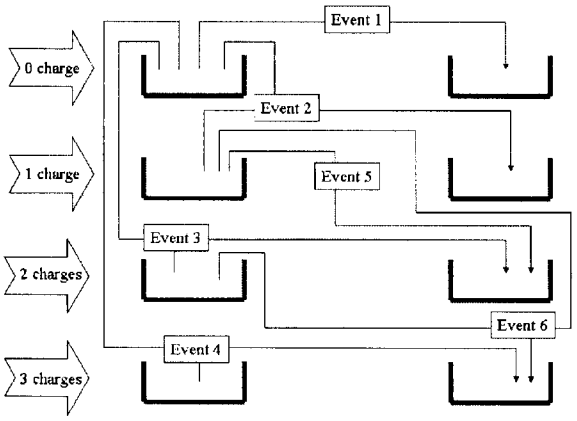

Figure 1. Model of coagulation of neutral-neutral, neutral-charged, and charged-charged (like-charged) particles

Derivation of Equations

Equations for the coagulation of neutral-neutral, neutral-charged, and like-charged particles are as follows, and will be discussed below:

$$\frac{dn_i}{dt} = -vdw \cdot \beta_{i,j} \cdot n_i \cdot n_j - nc01 \cdot \beta_{i,l} \cdot n_i \cdot n1_l - nc02 \cdot \beta_{i,l} \cdot n_i \cdot n2_l - nc03 \cdot \beta_{i,l} \cdot n_i \cdot n3_l \quad (1)$$

$$\frac{dn_j}{dt} = -vdw \cdot \beta_{i,j} \cdot n_i \cdot n_j \quad (2)$$

$$\frac{dn_k}{dt} = vdw \cdot \beta_{i,j} \cdot n_i \cdot n_j \quad (3)$$

$$\frac{d(n1_l)}{dt} = -nc01 \cdot \beta_{i,l} \cdot n_i \cdot n1_l - cc11 \cdot \beta_{l,j} \cdot n1_l \cdot n1_j - cc12 \cdot \beta_{l,l'} \cdot n1_l \cdot n2_{l'} \quad (4)$$

$$\frac{d(n2_l)}{dt} = -nc02 \cdot \beta_{i,l} \cdot n_i \cdot n2_l - cc12 \cdot \beta_{l,l'} \cdot n1_l \cdot n2_{l'} \quad (5)$$

$$\frac{d(n1_k)}{dt} = nc01 \cdot \beta_{i,l} \cdot n_i \cdot n1_l \quad (6)$$

$$\frac{d(n2_k)}{dt} = nc02 \cdot \beta_{i,l} \cdot n_i \cdot n2_l + cc11 \cdot \beta_{l,j} \cdot n1_l \cdot n1_j \quad (7)$$

$$\frac{d(n3_l)}{dt} = -nc03 \cdot \beta_{i,l} \cdot n_i \cdot n3_l \quad (8)$$

$$\frac{d(n3_k)}{dt} = nc03 \cdot \beta_{i,l} \cdot n_i \cdot n3_l + cc12 \cdot \beta_{l,l'} \cdot n1_l \cdot n2_{l'} \quad (9)$$

$$\frac{dn1_j}{dt} = -cc11 \cdot \beta_{l,j} \cdot n1_l \cdot n1_j \quad (10)$$

where, $1 \le i \le M$, $i \le j \le M$, $v_k = v_i + v_j$, $v1_k = v_i + v1_l$, $v2_k = v1_l + v1_{l'}$, $v2_k = v_i + v2_l$, $v3_k = v_i + v3_l$, $v3_k = v1_l + v2_{l'}$, $1 \le l \le M$, $1 \le l' \le M$.

M is the number of section bins; n_i is the number of neutral particles in size bin i; $n1_i$ is the number of charged particles with one charge in size bin i; $n2_i$ is the number of charged particles with two charges in size bin i; $n3_i$ is the number of charged particles with three charges in size bin i; v is the volume of neutral particle; v1 is the volume of charged particle with one charge; v2 is the volume of charged particle with two charges; v3 is the volume of charged particle with three charges; β is the collision frequency; *nc* is the enhancement factor between neutral-charged particles; *cc* is the enhancement factor between charged-charged particles; *vdw* is the enhancement factor due to van der Waals force only.

Equation 1 represents the decrease of neutral particles in size bin i due to the coagulation events 1, 2, 3, and 4. Equation 2 represents the decrease of neutral particles in size bin j due to the coagulation event 1. Equation 3 represents the increase of neutral particles in size bin k due to the coagulation event 1. Equation 4 represents the decrease of particles with one charge in size bin l due to the coagulation events 2, 5, and 6. Equation 5 represents the decrease of particles with two charges in size bin l due to the coagulation events 3 and 6. Equation 6 represents the increase of particles with one charge in size bin k due to the coagulation event 2. Equation 7 represents the increase of particles with two charges in size bin k due to the coagulation events 3 and 5. Equation 8 represents the decrease of particles with three charges in size bin l due to the coagulation event 4. Equation 9 represents the increase of particles with three charges in size bin k due to the coagulation events 4 and 6. Equation 10 represents the decrease of particles with one charge in size bin j due to the coagulation event 5.

The computation of the enhancement factors is based on the methodology in [20, 21].

Results and Discussion

The neutral-neutral particle collision rate is enhanced because of van der Waals forces. The neutral-charged particle collision rate is enhanced because of the combined van der Waals force and the electric image force. For the collision of like-charged particles, the

attractive forces of van der Waals and image forces and the repulsive Coulomb force have to be considered simultaneously. The computation of the enhancement factors follows the approach of Huang et al. [20,21].

Figure 2 shows the enhancement factors between neutral particles and charged particles with one charge only. Figure 3 shows the enhancement factors between neutral particles and the charged particles with two charges. Figure 4 shows the enhancement factors between neutral particles and the charged particles with three charges. It can be seen from Figures 2 to 4 that the image forces affect only the coagulation of small particles. The enhancement factor increases when the particle charges increase. The enhancement factor for large particles is almost the same for all three cases, and this is due to the fact that the charge in a large particle tends to be smeared so that the nature of neutral-charged particle interactions is similar to the neutral-neutral particle interactions.

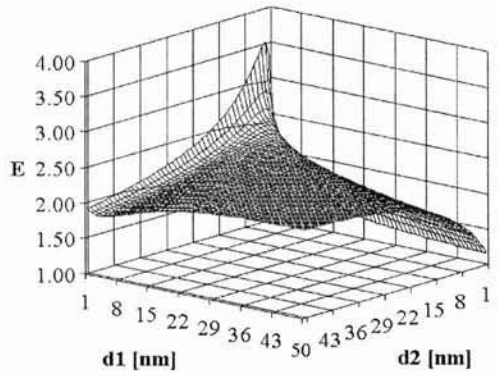

Figure 2. The enhancement factor for neutral-charged particle collision as a function of particle diameters (d1 denotes the charged-particle diameter with one charge, d2 denotes the neutral-particle diameter)

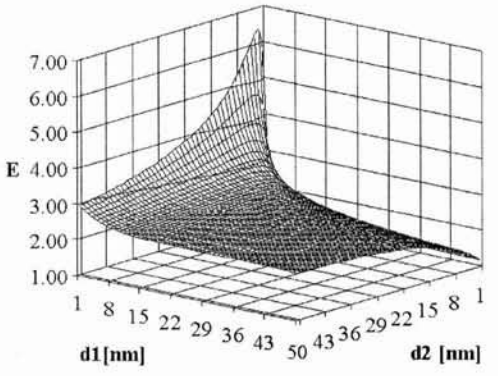

Figure 3. The enhancement factor for neutral-charged particle collision as a function of particle diameters (d1 denotes the charged-particle diameter with two charges, d2 denotes the neutral-particle diameter)

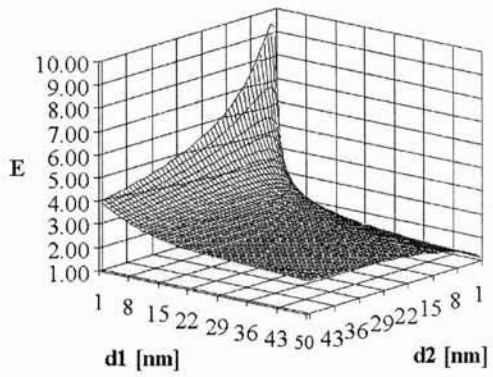

Figure 4. The enhancement factor for neutral-charged particle collision as a function of particle diameters (d1 denotes the charged-particle diameter with three charges, d2 denotes the neutral-particle diameter)

The coagulation of like-charged particles is retarded due to the Coulomb repulsive force between particles. The computation of the enhancement factor of like-charged particles is done by simultaneously considering the van der Waals, Coulomb and image forces. Figure 5 shows the enhancement factor between like-charged particles with one charge only. Figure 6 shows the enhancement factor between one-charge and two-charge particles. It can be seen from Figures 5 and 6 that the retardation of the coagulation is significant for small particles. If one particle is small and the other particle is very large, the increasing image force increases the enhancement factor.

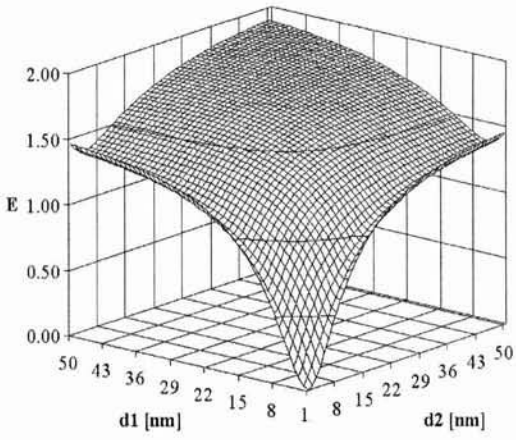

Figure 5. The enhancement factor for like-charged particle collision as a function of particle diameters (d1 and d2 denotes charged-particle diameters, one charge)

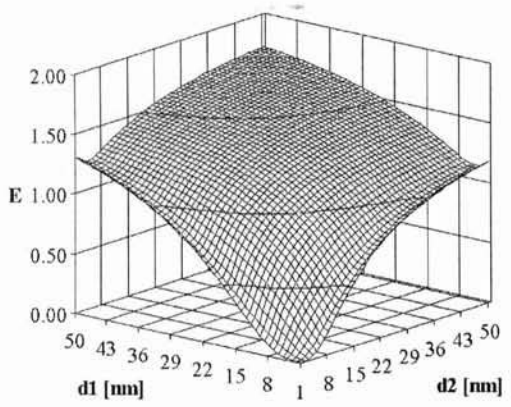

Figure 6. The enhancement factor for like-charged particle collision as a function of particle diameters (d1 denotes one-charge-particle diameters, d2 denotes two-charge-particle diameters)

The sectional method was used in the simulation code with 49 size bins for each component. The computer code allows any number of size bins and any type of initial particle size distributions. The code was used to predict the experimental data reported in [2].

Haynes et al. [2] measured soot particle number and size evolution in premixed flames with and without metal additives, as shown in Figure 6 of reference [2]. The simulation of Flame 3 in reference [2] starts with a monodispersed soot particle number density of 3E+11 /cm^3 and a diameter of 5.5 nm, which corresponds to the soot volume fraction of 2.62E-8 as shown in Table 1 of reference [2]. The simulated duration of soot particle evolution is the same as the measurement, which is 25 ms. The soot growth has been incorporated into the simulation, with the growth rate calculated from the measurement of soot volume fraction at the end of 25 ms to be 8.10E-8 for the unseeded flame and 6.24E-8 for the seeded flame (with 0.1 M K atomizer solution).

Figure 7 shows the simulation of the soot particle coagulation for the unseeded flame (without soot particle charging). At the end of 25 ms, the simulation results show the soot particle number density to be 3.581E+9 /cm^3, and the geometric mean particle diameter to be 33.43 nm with geometric standard deviation of 1.22. This result is very close to the measurements with particle number density of about 3.9E+9 /cm^3 and particle diameter of about 39 nm as shown in Figure 6 of reference [2]. The number mean diameter is 33.10 nm, and the relative standard deviation (standard deviation / number mean diameter) $\sigma = 0.20$.

Theoretical analysis [23] suggests that a self-preserving size distribution will form after a long time of coagulation regardless of the initial particle size distribution, and this self-preserving size distribution is approximately lognormal with a geometric standard deviation of about 1.32 to 1.36. Thus, at the end of 25 ms, the soot particles has not been evolved into a self-preserving particle size distributions at the end of 25 ms.

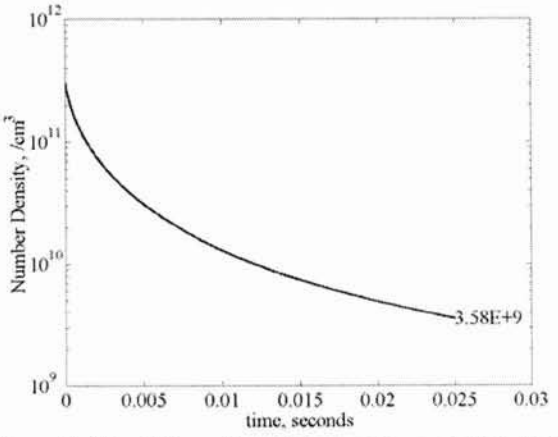

Figure 7. Simulation of particle number evolution for the case of no metal additives.

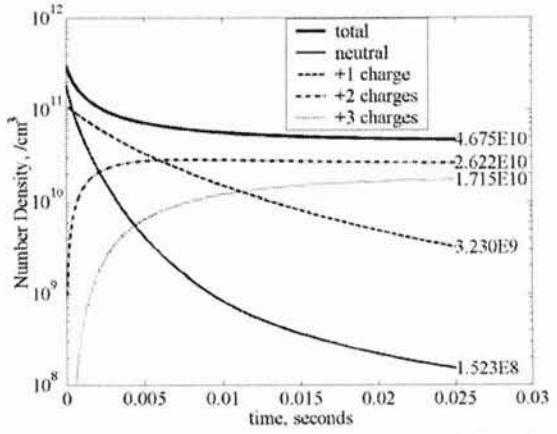

Figure 8. Simulation of particle number evolution for the case of 0.1 M metal additives.

Figure 8 shows the simulation of the soot particle coagulation for seeded flame. At the end of 25 ms the simulation results shows the total soot particle number density to be 4.675E+10 /cm^3, and the geometric mean particle diameter to be 13.22 nm with a geometric standard deviation of 1.18. This is also very close to the measurements with the particle number density of about 5.0E+10 /cm^3 and the particle diameter of about 13.7 nm as shown in Figure 6 of reference [2]. The number mean diameter is 13.37 nm, and the relative standard deviation is 0.16. Comparing with the unseeded flame simulation, the results show that by charging the soot particles with metal additives, the coagulation has been impeded and results in higher soot particle number density with smaller particle diameter.

The simulation results for the seeded flame shows that approximately 38% of the soot particles are charged assuming that the charging process occurs before the soot particles have grown to 5.5 nm and that all charged particles have one charge at this point. After 25 ms, the majority of the soot particles have been charged due to the coagulation of neutral particles with charged particles. At the end of 25 ms, 56% of the particles (number count) have two charges, 37% particles have three charges, 7% particle have one charges, and only 0.33% particles remain neutral.

The predicted particle size distribution at the end of 25 ms for the unseeded flame is shown in Figure 9. It can be seen that the particle size distribution has evolved into a lognormal distribution due to the coagulation process.

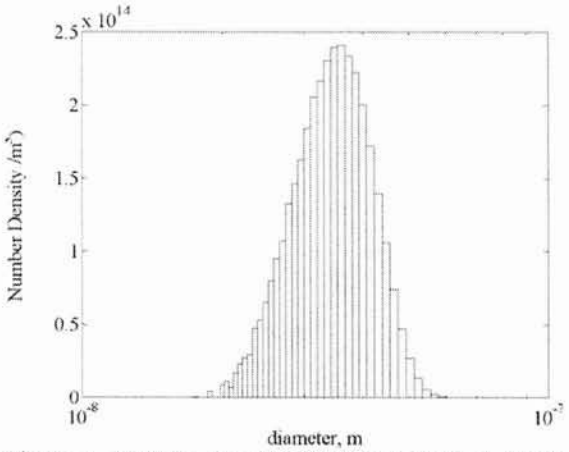

Figure 9. Particle size distribution at the end of 25 ms coagulation process of neutral particles

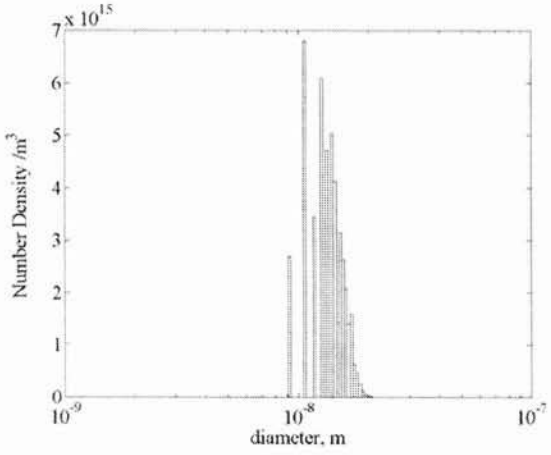

Figure 10. Particle size distribution at the end of 25 ms coagulation process of charged soot particles

The particle size distribution for the charged particles at the end of the 25 ms coagulation process is shown in Figure 10. As shown, the particle size distribution has not evolved into lognormal size distribution, the result of the reduction in the collision rate by repulsive Coulomb forces.

The soot particle number and size measurements done by Haynes [2] was based on the assumption of a monodispersed particle size, and measuring the light scattering and absorption simultaneously. The scatter factor for monodispersed particles in the Rayleigh regime is given by

$$Q_{vv} = \left(\frac{2\pi}{\lambda}\right)^4 \left|\frac{m^2-1}{m^2+2}\right|^2 N_{mono} r_{mono}^6 \tag{11}$$

The extinction coefficient, k_{ext}, is given by

$$k_{ext} = -\left(\frac{8\pi^2}{\lambda}\right) \mathrm{Im}\left(\frac{m^2-1}{m^2+2}\right) N_{mono} r_{mono}^3 \tag{12}$$

where, m is the refractive index of soot particles, and λ is the light wavelength.

Solving the equations 11 and 12 simultaneously, we can obtain the monodispersed total particle number and diameter.

From the computer simulation results, we have particle size distribution information. Thus, we can relate the particle number and diameter between monodispersed and polydispersed cases. From the particle scatter factor formulation (Equation 11), we have:

$$\sum n_i r_i^6 = N_{mono} r_{mono}^6 \tag{13}$$

From Equation 12, we have:

$$\sum n_i r_i^3 = N_{mono} r_{mono}^3 \tag{14}$$

With the information of n_i and r_i given from the simulation results, by solving Equations 13 and 14 simultaneously we can obtain N_{mono} and r_{mono}. For the unseeded flame as shown in Figure 9, we have N_{mono} = 2.67E+9, d_{mono} = 38.95 nm. The ratio between polydispersed and monodispersed particle number, N/N_{mono} = 1.34. The simulation showed the number mean diameter is 33.10 nm and the geometric mean diameter is 33.43 nm. The ratio of the geometric mean diameter to the monodispersed diameter, d/d_{mono} = 0.86. The relative standard deviation σ = 0.20.

The above ratios are closer to unity for the case of the seeded flame. In this case, N/N_{mono} = 1.21, and d/d_{mono} = 0.90.

The above results indicate that the monodisperse approximation overestimated the particle diameter and underestimated the particle number.

Conclusions

Model and equations for the coagulation of charged particles were developed. The model includes neutral particles and charged particles (up to three charges). The

enhancement factors for the coagulation between neutral and charged particles, and between like-charged particles, have been computed. These factors have been used in a computer code for simulating the coagulation of charged particles. The enhancement factors for the collision of neutral-charged particles and the collision of like-charged particles were computed. The enhancement factor for the like-charged particles is very small for particles with small diameters.

The simulation results show that, for the seeded flame [2], about 38% of the soot particles are charged at the point where soot particles are 5.5 nm in diameter. Through the 25 ms coagulation process, the particles with two charges dominate the number density (56%). The neutral particle number density dropped from 62% to 0.33%. Particles with one charge represent 7%, and the particles with three charges represent 37%.

The simulation results showed a lognormal particle size distribution for the unseeded flame, and the geometric mean diameter was 33.43 nm with a geometric standard deviation of 1.22. The like-charged particle collision rate was reduced due to the Coulomb repulsive force, thus the particle size distribution for the seeded flame had not yet evolved into a lognormal size distribution. The coagulation of like-charged particles lead to a geometric mean diameter of 13.22 nm with a geometric standard deviation of 1.18.

The comparison between monodispersed and polydispersed particle size distributions indicated that for the unseeded flame $N/N_{mono} = 1.34$, $d/d_{mono} = 0.86$, and the relative standard deviation is 0.20; and for the seeded flame, $N/N_{mono} = 1.21$, $d/d_{mono} = 0.90$, and the relative standard deviation is 0.16.

Acknowledgements

This project is supported by the Strategic Environmental Research and Development Program, Department of Defense, Department of Energy and the Environmental Protection Agency (SERDP) and the Department of Energy, Accelerated Strategic Computing Initiative (ASCI) for the Center for the Simulation of Accidental Fires and Explosions (C-SAFE).

References

1. J. Lawton, F.J. Weinberg, Electrical Aspects of Combustion. Oxford University Press, 1969, p.229
2. B.S. Haynes, H. Jander, H.GG. Wagner, Seventeenth Symposium (International) on Combustion, The Combustion Institute, Pittsburgh, 1979, pp.1365-1374
3. A.N. Hayhurst, H.R.N. Jones, Combust. Flame 78 (1989) 339-356
4. J.B.A. Mitchell, D.J.M. Miller, Combust. Flame 75 (1989) 45-55
5. V.J. Hall-Roberts, A.N. Hayhurst, D.E. Knight, S.G. Taylor, Combust. Flame 120 (2000) 578-584
6. K.C. Salooja, Nature 240 (1972) 350-351
7. E.M. Bulewicz, D.G. Evans, P.J. Padley, Fifteenth Symposium (International) on Combust, The Combustion Institute, Tokyo, 1974, pp.1461-1470
8. R.J. Bowser, F.J. Weinberg, Nature 249 (1974) 339-340
9. A. Feugier, Symposium on Evaporation-combust of Fuel Droplets, San Francisco, 1976, pp.211-218
10. R. Wegert, W. Wiese, K.H. Homann, Combust. Flame 95 (1993) 61-75
11. B.L. Wersborg, A.C. Yeung, J.B. Howard, Fifteenth Symposium (International) on Combust, The Combustion Institute, Tokyo, 1974, pp.1439-1448
12. A.A. Onischuk, S. di Stasio, V.P. Strunin, V.V. Karasev, A.V. Baklanov, V.N. Panfilov, Journal of Aerosol Science 31 (SUPPL.1) (2000) S948-S949
13. H. Ohisa, H. Horisawa, I. Kimura, Transactions of the Japan Society of Mechanical Engineers, Part B, 63 (611) (1997) 2515-2522
14. H. Ohisa, I. Kimura, H. Horisawa, Combust. Flame 116 (1999) 653-661
15. M. Balthasar, F. Mauss, Combust. Flame 129 (2002) 204-216
16. J.B. Howard, B.L. Wersborg, G.C. Williams, Faraday Symposia of the Chemical Society 7 (1973) 109-119
17. R.T. Ball, J.B. Howard, Thirteenth Symposium (International) on Combustion, The Combustion Institute, Pittsburgh, 1970, pp.353-362
18. H.J. Mick, A. Hospital, P. Roth, Journal of Aerosol Science 22 (1991) 831-841
19. P. Roth, A. Hospital, Twenty-Fourth Symposium (International) on Combustion, The Combustion Institute, Pittsburgh, 1992, pp.981-989
20. D.D. Huang, J.H. Seinfeld, W.H. Marlow, Journal of Colloid and Interface Science 140 (1990) 258-276
21. D.D. Huang, J.H. Seinfeld, K. Okuyama, Journal of Colloid and Interface Science 141 (1991) 191-198
22. P. Jiang, J.S. Lighty, A.F. Sarofim, E.G. Eddings, L.J. Xu, G.R. Paetow, E.L. Douglas, 21st Annual AAAR Conference, October 7-11, 2002, Charlotte, North Carolina
23. W.C. Hinds, Aerosol Technology: properties, behavior, and measurement of airborne particles, John Wiley & Sons, New York, USA, 1999, pp.271-273